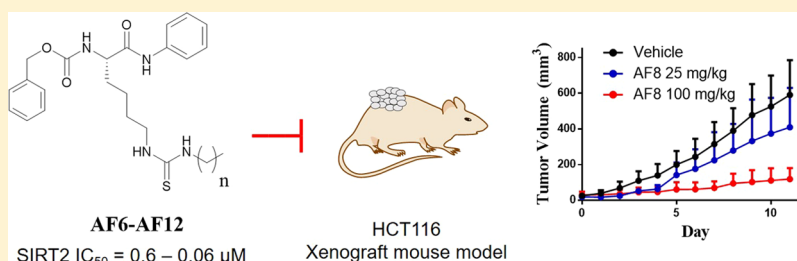


## Novel Lysine-Based Thioureas as Mechanism-Based Inhibitors of Sirtuin 2 (SIRT2) with Anticancer Activity in a Colorectal Cancer Murine Model

Ali Sohail Farooqi,<sup>†</sup> Jun Young Hong,<sup>†</sup> Ji Cao,<sup>†,§</sup> Xuan Lu,<sup>†</sup> Ian Robert Price,<sup>†</sup> Qingjie Zhao,<sup>†,||</sup> Tatsiana Kosciuk,<sup>†</sup> Min Yang,<sup>†</sup> Jessica Jingyi Bai,<sup>†</sup> and Hening Lin<sup>\*,†,§</sup><sup>†</sup>Department of Chemistry and Chemical Biology and <sup>‡</sup>Howard Hughes Medical Institute, Department of Chemistry and Chemical Biology, Cornell University, Ithaca, New York 14853, United States

## Supporting Information



**ABSTRACT:** Sirtuin 2 (SIRT2) is a protein lysine deacetylase that has been indicated as a therapeutic target for cancer. To further establish the role of SIRT2 in cancers, it is necessary to develop selective and potent inhibitors. Here, we report the facile synthesis of novel lysine-derived thioureas as mechanism-based SIRT2 inhibitors with anticancer activity. Compounds AF8, AF10, and AF12 selectively inhibited SIRT2 with  $IC_{50}$  values of 0.06, 0.15, and 0.08  $\mu\text{M}$ , respectively. Compounds AF8 and AF10 demonstrated broad cytotoxicity amongst cancer cell lines, but minimal toxicity in noncancerous cells. AF8 and AF10 inhibited the anchorage-independent growth of human colorectal cancer cell line HCT116 with  $GI_{50}$  values of  $\sim 7 \mu\text{M}$ . Furthermore, AF8 potently inhibited tumor growth in a HCT116 xenograft murine model, supporting that SIRT2 is a viable therapeutic target for colorectal cancer.

## INTRODUCTION

Sirtuins are a class of nicotinamide adenine dinucleotide ( $\text{NAD}^+$ )-dependent enzymes with lysine deacetylase activities.<sup>1,2</sup> They are also referred to as class III histone deacetylases, but can catalyze the deacetylation of various nonhistone substrates.<sup>3</sup> In mammals, there are seven sirtuins (SIRT1–7) that are involved in the regulation of cellular metabolism, transcription, and differentiation.<sup>4,5</sup> Specifically, SIRT1, SIRT2, and SIRT5 have been implicated in promoting cancer cell proliferation and tumorigenesis.<sup>6–8</sup> While SIRT1 and SIRT2 have also been contradictorily shown to be tumor suppressors,<sup>7,9</sup> the therapeutic potential of targeting SIRT2 has been demonstrated by isoform specific inhibition in breast cancer cell lines.<sup>10</sup> Recently, SIRT2 was shown to promote tumor growth by regulating oncogenes *c-Myc* and *KRas*.<sup>6,11</sup> SIRT2 also promotes basal-like breast cancer phenotype and tumor growth through the deacetylation and stabilization of transcription factor Slug.<sup>12</sup> As such, SIRT2 regulates multiple oncogenic pathways and is a promising therapeutic target for cancer. However, there is a need for more studies in animal models of cancer to convincingly demonstrate the therapeutic potential of SIRT2 inhibition.

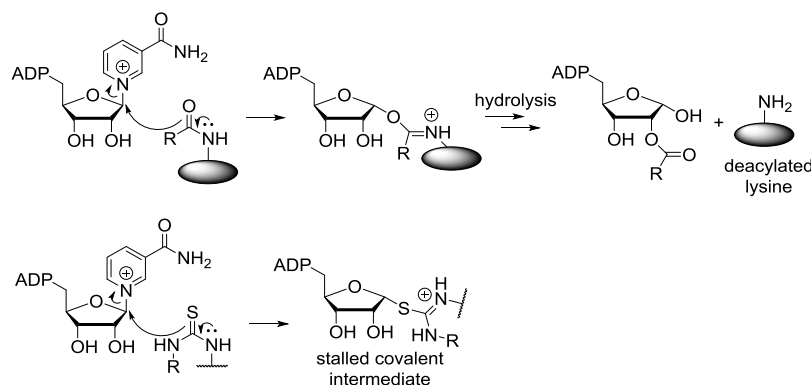
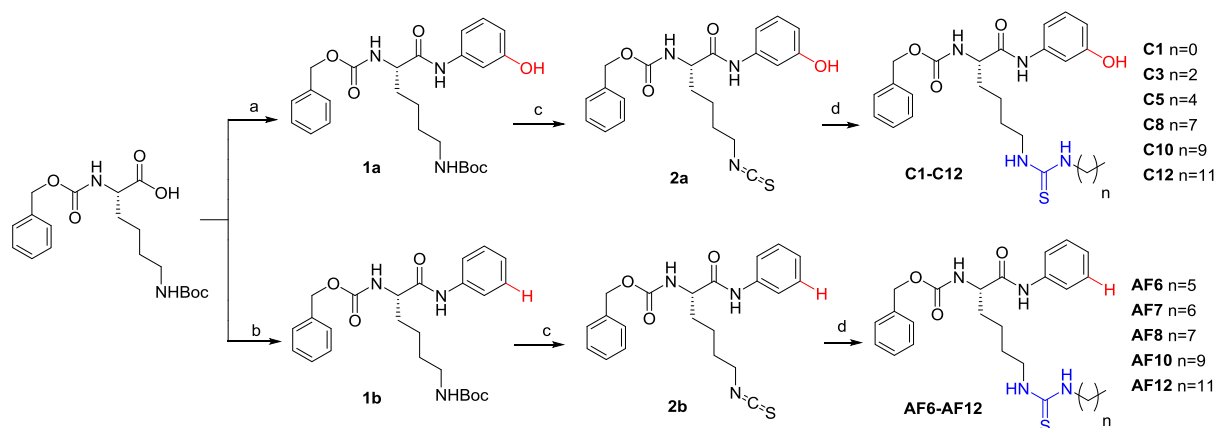
Several SIRT2-selective inhibitors, such as AGK2, tenovin-6, TM, and SirReal2, have been reported.<sup>10,13–15</sup> Among these,

the thiomristoyl lysine compound TM is a SIRT2 mechanism-based inhibitor that displayed cancer cell-selective toxicity and is active in many human cancer cell lines.<sup>10,16</sup> The sirtuin deacetylation mechanism involves nucleophilic attack on the  $\text{NAD}^+$  anomeric position by the carbonyl of the acyl group to release nicotinamide (Scheme 1).<sup>17</sup> TM contains a thiomristoyl lysine moiety, which can attack the anomeric position of  $\text{NAD}^+$  in the presence of SIRT2, forming a stable covalent intermediate to potently inhibit SIRT2.<sup>10</sup>

While TM has promising anticancer activity, it is poorly soluble in water and the synthesis of the thioamide bond is difficult and results in poor yield. We therefore sought to develop similar mechanism-based inhibitors that are less hydrophobic and easier to synthesize. In a previous study by Hirsch et al., it was shown that a peptidomimetic thiourea-containing compound could mechanistically inhibit SIRT1 and lead to the general inhibition of SIRT1–3.<sup>18</sup> Modifying TM with a thiourea moiety could similarly result in mechanism-based inhibition and facilitate a simplified synthesis route. Here, we present the development of novel lysine-based thioureas as potent and selective SIRT2 inhibitors with

Received: January 30, 2019

Scheme 1. Inhibition of Sirtuin Lysine Deacylation by Thiourea Compounds

Scheme 2. Synthesis of Thiourea Compounds with Varying Chain Lengths<sup>a</sup>

<sup>a</sup>Reactions and conditions: (a) (i) dichloromethane (DCM), N-methylmorpholine, isobutyl chloroformate, 1 h; (ii) 3-aminophenol, 16 h. (b) (i) DCM, N-methylmorpholine, isobutyl chloroformate, 1 h; (ii) aniline, 16 h. (c) (i) DCM/trifluoroacetic acid, 1 h; (ii) tetrahydrofuran, triethylamine (TEA), 1,1'-thiocarbonyldiimidazole, 16 h. (d) dimethylformamide, TEA, corresponding primary alkylamine, 16 h.

anticancer activity in various cancer cell lines and a colorectal cancer xenograft murine model.

## RESULTS AND DISCUSSION

**Design and Synthesis of New SIRT2 Inhibitors.** Two different classes of thiourea inhibitors with varying alkyl chain lengths were synthesized through a divergent synthesis route (Scheme 2). The C class of inhibitors C1–12 contained a 3' hydroxyl group on the C-terminal while the AF class of inhibitors AF6–12 did not. Modeling the inhibitors into the known SIRT2 structure suggested the 3' hydroxyl group of the C inhibitors could facilitate additional hydrogen bonding interactions with the backbone of residues Val266 or Gln267 (Figure 1).<sup>19</sup> The C inhibitors could therefore have improved potency and solubility as compared to the AF inhibitors. SIRT2 contains a hydrophobic pocket for acyl group binding,<sup>15,20</sup> and this pocket accommodates the thiomristoyl group present in TM. Toward the goal of reducing the hydrophobicity of the inhibitors, we decided to synthesize thiourea compounds with various alkyl chain lengths.

Commercially available Cbz-L-lysine(Boc)-OH was converted to the corresponding isothiocyanate intermediates 2a and 2b in two steps with 54% and 83% yield, respectively. The isothiocyanate compounds were then coupled with varying alkyl chain primary amines to form the resultant thiourea compounds, with up to 94% yield. In total, the six C1–C12

inhibitors varied in chain length from one to 12 carbons and the five AF6–AF12 inhibitors varied from six to 12 carbons.

**AF8, AF10, and AF12 are Potent and Selective SIRT2 Inhibitors in Vitro.** We then measured the ability of these compounds to inhibit SIRT1, SIRT2, and SIRT3. Because SIRT1, SIRT2, and SIRT3 are similar structurally and comprise the class I sirtuins,<sup>21</sup> it was important to test for selectivity among these three isoforms. A liquid chromatography (LC)-based assay with acetyl H3K9 peptide<sup>2</sup> and purified sirtuins was used to test the compounds for SIRT1–3 inhibition. The previously reported TM compound was also assayed and used as a reference compound. Nicotinamide, a nonspecific sirtuin inhibitor, was used as a positive control for SIRT3 inhibition and the SIRT1 selective inhibitor EX527 used as a positive control for SIRT1 inhibition.<sup>22–24</sup> Nicotinamide weakly and nonspecifically inhibited SIRT3 ( $IC_{50}$   $76 \pm 30 \mu\text{M}$ ) and SIRT2 ( $IC_{50}$   $70 \pm 5 \mu\text{M}$ ) while EX527 more potently inhibited SIRT1 ( $IC_{50}$   $0.085 \pm 0.01 \mu\text{M}$ ) over SIRT2 ( $IC_{50}$   $1.80 \pm 0.03 \mu\text{M}$ ), consistent with reported literature values.<sup>22,25</sup>

As shown in Table 1, none of the synthesized inhibitors demonstrated significant inhibition of SIRT3 with  $IC_{50}$  values of  $50 \mu\text{M}$  or greater. Except for inhibitors C1 and C3, all inhibitors had micromolar (C5) or submicromolar  $IC_{50}$  values for SIRT2. The lack of SIRT2 deacetylase inhibition for compounds C1 and C3 is likely because of the shorter side chains of one and three carbons, respectively, which led to

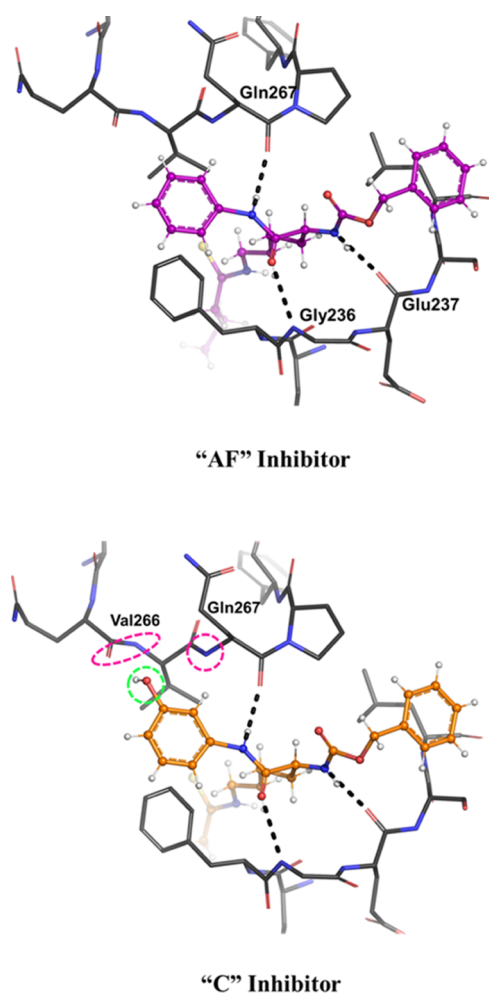


**Figure 1.** C class inhibitors modeled into the peptide-binding site of SIRT2 (PDB code 4X3O) show additional possible hydrogen bonds as compared to the AF inhibitors. For both classes of inhibitors, hydrogen bonds are predicted to form between the lysine carbonyl and the Gly236 backbone nitrogen, between the *N*-terminus lysine backbone nitrogen and the Glu237 backbone carbonyl, and between the *C*-terminus backbone nitrogen and the Gln267 backbone carbonyl. The 3' hydroxyl of the C class inhibitors (circled in green) could make additional hydrogen bonds with the Gln267 backbone nitrogen or the Val266 backbone carbonyl or nitrogen (circled in pink).

decreased interactions in the sirtuin hydrophobic pocket. A trend of increased chain length and increased SIRT2 inhibition was observed, suggesting that a longer alkyl chain length facilitates increased binding in the hydrophobic pocket.

Compounds **C8–C12** were potent for SIRT2 with  $IC_{50}$  values of 0.12  $\mu\text{M}$  or lower, but also inhibited SIRT1 with  $IC_{50}$  values of 1.0, 0.45, and 1.0  $\mu\text{M}$  for **C8**, **C10**, and **C12**, respectively. The decreased selectivity is likely because the additional hydrogen bonding capability of **C8–C12** increases the SIRT1 inhibition more than the SIRT2 inhibition. The resultant 8 to 17-fold selectivity for SIRT2 over SIRT1 was not adequate to ensure SIRT2-specific inhibition for biological testing. As a result, the nonselective inhibitors **C8–C12** were not used in further biological activity assays.

**AF6**, **AF7**, **AF8**, **AF10**, and **AF12** inhibited SIRT2 deacetylase activity with  $IC_{50}$  values of 0.64, 0.16, 0.061, 0.15, and 0.081  $\mu\text{M}$ , respectively (Table 1). **AF8** slightly inhibited SIRT1 deacetylase activity ( $IC_{50}$  11  $\pm$  5  $\mu\text{M}$ ) while

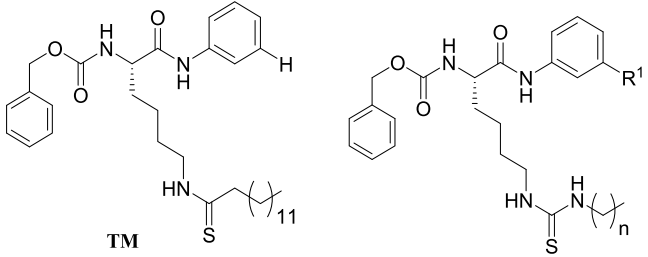
**AF10**, **AF12**, and **TM** showed no inhibition of SIRT1. The inhibition of SIRT3 was the weakest and only **AF8** showed slight inhibition of SIRT3. The selectivity for SIRT2 over SIRT1 correlated with the alkyl chain length of the inhibitors, as demonstrated by the 47, 137, 180, >1000, and >1000-fold selectivity of **AF6**, **AF7**, **AF8**, **AF10**, and **AF12**, respectively. This trend suggests that longer alkyl chains can exploit isoform specific binding for selective SIRT2 inhibition, despite the fact that SIRT1–3 have similar hydrophobic acyl pockets.<sup>26</sup> **AF8** inhibition of SIRT2 ( $IC_{50}$  0.061  $\pm$  0.03  $\mu\text{M}$ ) was the most potent amongst the thiourea inhibitors and comparable to **TM** ( $IC_{50}$  0.034  $\pm$  0.01  $\mu\text{M}$ ).

**AF8** was confirmed to work through mechanism-based inhibition of SIRT2. **AF8** was incubated with an excess of SIRT2 and  $\text{NAD}^+$  and the reaction mixture analyzed by LC–mass spectrometry (MS). As shown in Figure 2, the covalent **AF8**-ADP-ribose intermediate formed by the release of nicotinamide was detected. When **AF8** was removed from the reaction mixture, the intermediate mass was not detected. This result confirmed that **AF8**, and likely the other thiourea **AF** inhibitors, could covalently react with  $\text{NAD}^+$ . This is consistent with the MS detection of the stalled *S*-alkylamide intermediate of a previously reported, nonspecific lysine-based thiourea sirtuin inhibitor upon incubation with SIRT1.<sup>18</sup>

**AF8** and **AF10** Demonstrated Cytotoxicity Against Human Colon, Lung, Breast, and Pancreatic Cancer Cell Lines. The thiourea modification and shorter alkyl chains of compounds **AF10** and **AF8** were predicted to improve solubility as **TM** had a calculated  $c\text{Log}P$  value of 8.8, while the thiourea analogues **AF10** and **AF8** had calculated  $c\text{Log}P$  values of 7.04 and 6.13, respectively (Table 1). Thus, the lower  $c\text{Log}P$  values suggest that **AF8** and **AF10** may have improved solubility while still maintaining reasonable selectivity and potency for SIRT2. Because of this, **AF8** and **AF10** were tested for possible anticancer activity amongst various cell lines.

As shown in Table 2, toxicity was observed in all cancer lines upon treatment with **AF8**, **AF10**, and **TM**. None of the inhibitors were toxic to noncancerous HME1 epithelial cells. In a normal colon cell line, CCD 841 CoN, the  $GI_{50}$  values of **AF8** and **AF10** were also higher in general than those in the cancer cell lines tested. These observations suggested that, while there is variation, cancer cells could rely more on SIRT2-driven pathways for survival and growth. **AF10** was the most potent inhibitor and was approximately two-fold more potent than **TM** in MCF7, MDA-MB-231, A549, SW948, and HCT116 cells (Table 2). **AF8** was comparable to **TM** in most cell lines except the pancreatic BxPC-3 cell line, which showed little inhibition by **AF8**. Both **AF8** and **AF10** were twice as potent in the colorectal HCT116 cell line as compared to **TM** (Table 2). **AF8** demonstrated minimal inhibition of noncancerous colon cell line CCD 841 CoN, suggesting that **AF8** could be used to selectively target cancerous colon cells. Consistent with its increased potency, **AF10** showed higher toxicity in CCD 841 CoN cells, which indicated it may have a lower therapeutic index (Table 2).

**AF8**, **AF10**, and **TM** Inhibited the Anchorage-Independent Growth of HCT116 Cells. The ability of cancer cells to survive and proliferate without adhesion to an extracellular matrix is one of the hallmarks of oncogenic transformation.<sup>27,28</sup> To examine anchorage-independent growth, HCT116 cells were suspended in a soft agar matrix and incubated until colony growth was observed.<sup>29</sup> Slightly less overall growth was observed in the **TM** treated group, likely

Table 1. In Vitro IC<sub>50</sub> Values of Inhibitors for SIRT1-3 and Relative Selectivity for SIRT2 Over SIRT1


compound	R <sup>1</sup>	chain length	SIRT1 IC <sub>50</sub> (μM) <sup>a</sup>	SIRT2 IC <sub>50</sub> (μM)	SIRT3 IC <sub>50</sub> (μM)	SIRT2/SIRT1 selectivity	cLogP <sup>b</sup>
C1	OH	n = 0	>100	>100	>100	NA	2.65
C3	OH	n = 2	>100	>100	>100	NA	3.52
C5	OH	n = 4	34 ± 2	1.0 ± 0.3	>100	34	4.42
C8	OH	n = 7	1.0 ± 0.6	0.12 ± 0.001	>100	8	5.79
C10	OH	n = 9	0.45 ± 0.1	0.036 ± 0.0001	>100	12	6.7
C12	OH	n = 11	1.0 ± 0.6	0.060 ± 0.0005	>100	17	7.6
AF6	H	n = 5	30 ± 11	0.64 ± 0.02	68 ± 19	47	5.22
AF7	H	n = 6	22 ± 2	0.16 ± 0.006	83 ± 11	137	5.68
AF8	H	n = 7	11 ± 5	0.061 ± 0.030	51 ± 0.4	180	6.13
AF10	H	n = 9	>200	0.15 ± 0.06	>200	>1000	7.04
AF12	H	n = 11	>200	0.081 ± 0.030	>200	>1000	7.95
TM	NA	NA	>200	0.034 ± 0.010	>100	>1000	8.80
Nicotinamide	NA	NA		70 ± 5	76 ± 30		
EX527	NA	NA	0.085 ± 0.01	1.80 ± 0.03			

<sup>a</sup>In vitro IC<sub>50</sub> values were calculated in duplicate using acetylated H3K9 peptide and LC. Statistical analysis was done on GraphPad Prism, and reported values include the SEM. <sup>b</sup>cLogP values computed using DataWarriors software.

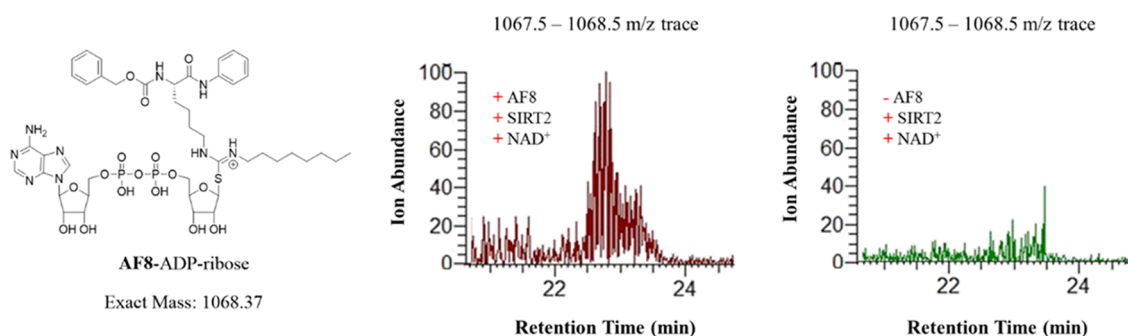


Figure 2. Detecting the covalent intermediate formed between AF8 and NAD<sup>+</sup> in the presence of SIRT2 by LC-MS. When AF8 was removed from the reaction mixture, the intermediate mass was not detected as shown through the 1067.5–1068.5 *m/z* ion trace.

Table 2. GI<sub>50</sub> Values of SIRT2 Inhibitors Across a Variety of Cell Lines

cell line	type	TM GI <sub>50</sub> (μM)	AF8 GI <sub>50</sub> (μM)	AF10 GI <sub>50</sub> (μM)
MCF7	breast cancer	37.0 ± 4.5	42.6 ± 18.5	18.4 ± 6.0
MDA-MB-468	breast cancer	15.7 ± 2.5	26.1 ± 6.4	13.4 ± 1.7
MDA-MB-231	breast cancer	42.8 ± 6.5	27.2 ± 8.1	14.8 ± 4.1
BxPC-3	pancreatic cancer	13.3 ± 3.5	72.4 ± 25.5	24.3 ± 5.0
NCI-H23	lung cancer	16.4 ± 1.8	35.8 ± 14.2	15.6 ± 3.5
A549	lung cancer	17.3 ± 6.0	20.8 ± 6.9	9.0 ± 3.9
SW948	colorectal cancer	19.2 ± 3.5	30.0 ± 8.9	12.8 ± 3.5
HCT116	colorectal cancer	131.6 ± 54.0	58.9 ± 26.5	54.4 ± 12.6
CCD 841 CoN	colon cells	n.d. <sup>a</sup>	136.8 ± 53.5	47.4 ± 7.0
HME1	epithelial cells	n.i. <sup>b</sup>	n.i.	n.i.

<sup>a</sup>n.d.: not determined. <sup>b</sup>n.i.: no inhibition.

because of a smaller number of cells seeded per well. Treatment with AF8 and AF10 potently inhibited colony formation with GI<sub>50</sub> values of 7.4 and 7.0 μM, respectively, while TM had a weaker effect with a GI<sub>50</sub> value of 16.7 μM

(Figure 3). The potency of the compounds in the soft agar colony formation assay shows that they can inhibit anchorage-independent growth better than normal 2D growth (cytotoxicity assay described in the previous section), suggesting that

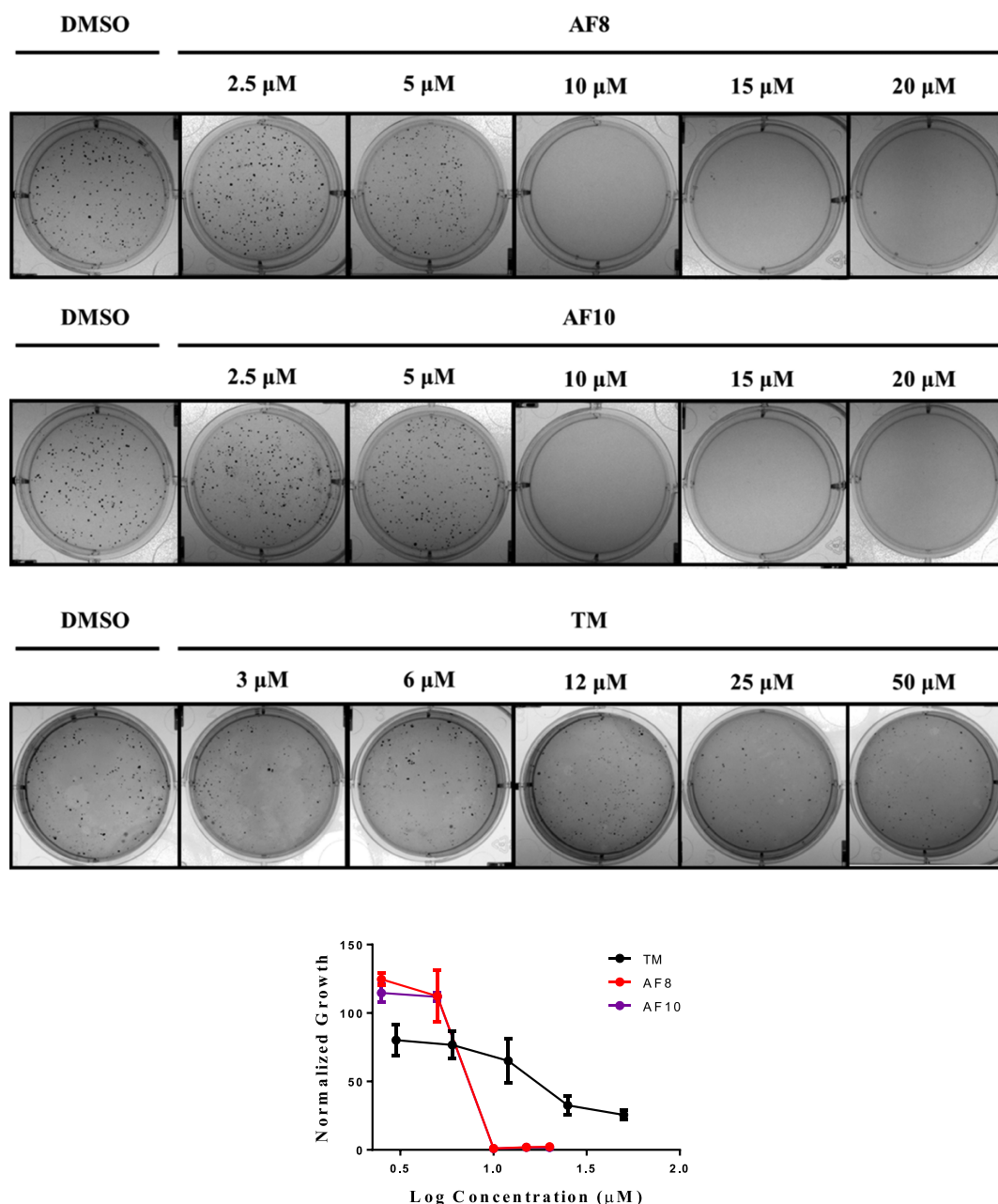


**Figure 3.** AF8, AF10, and TM inhibited the anchorage-independent growth of HCT116 cells in a soft agar colony formation assay. At a concentration of 10  $\mu\text{M}$  and greater, AF8 and AF10 completely inhibited the growth of HCT116 cells. The  $\text{GI}_{50}$  values for AF8 and AF10 were 7.4 and 7.0  $\mu\text{M}$ , respectively, whereas the  $\text{GI}_{50}$  for TM was 16.7  $\mu\text{M}$ .

SIRT2 inhibitors preferentially target the transformed phenotype of cancer cells. This is also consistent with the fact that the inhibitors exhibit less toxicity toward non-cancerous cells in the 2D growth assay shown in Table 2.

#### AF8 and AF10 Inhibit SIRT2 but Not SIRT1 in Cells.

We next sought to confirm that AF8 and AF10 could selectively inhibit SIRT2 deacetylase activity in cells. Compounds C3, C5, and C10 were also tested to determine if our in vitro sirtuin inhibition assay correlated with SIRT2 inhibition in cells. We monitored  $\alpha$ -tubulin acetylation as a readout for SIRT2 inhibition as  $\alpha$ -tubulin is a well-known SIRT2 deacetylation substrate.<sup>30</sup> HCT116 cells were incubated with dimethylsulfoxide (DMSO) alone (control) or varying concentrations of inhibitor for 6 h before  $\alpha$ -tubulin acetylation was detected by immunofluorescence. As shown in Figure

4A,C, acetyl  $\alpha$ -tubulin levels of HCT116 cells increased upon treatment with TM at 25 and 50  $\mu\text{M}$ , suggesting the inhibition of SIRT2 activity. AF8 and AF10 treatment at 25 and 50  $\mu\text{M}$  also resulted in extensive  $\alpha$ -tubulin hyperacetylation as compared to DMSO. Thus, AF8 and AF10 can also inhibit SIRT2 activity in cells.

SIRT2 inhibition in cells as measured by  $\alpha$ -tubulin acetylation was consistent with calculated in vitro SIRT2 inhibition results. As shown in Figure 4B,D, treatment with 25 or 50  $\mu\text{M}$  of C3 did not increase the acetylation of  $\alpha$ -tubulin, corroborating the lack of in vitro SIRT2 inhibition ( $\text{IC}_{50} > 100 \mu\text{M}$ ). C5 slightly increased  $\alpha$ -tubulin acetylation at 25  $\mu\text{M}$  and more robustly increased acetylation at 50  $\mu\text{M}$ , consistent with moderate in vitro SIRT2 inhibition ( $\text{IC}_{50}$  1.0  $\mu\text{M}$ ). C10 increased  $\alpha$ -tubulin acetylation at both 25 and 50  $\mu\text{M}$ ,

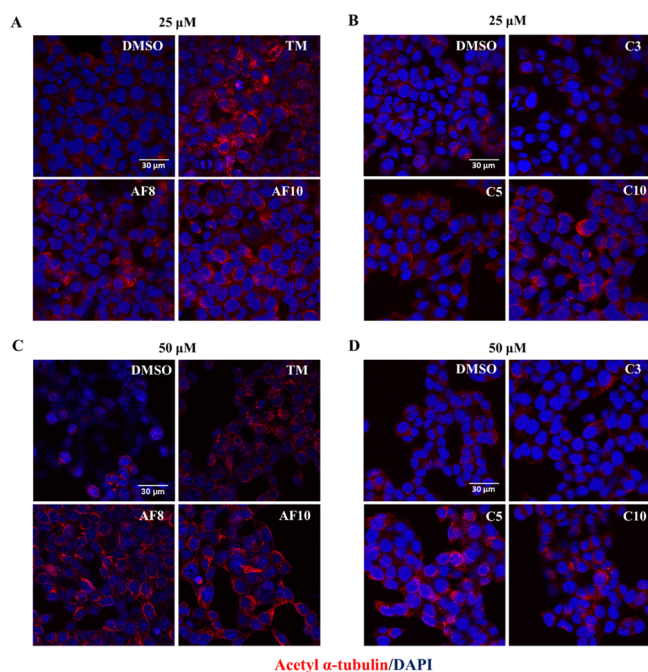


**Figure 4.** AF8, AF10, TM, C5, and C10 inhibit SIRT2 activity in HCT116 cells as shown through an increase in  $\alpha$ -tubulin acetylation. HCT116 cells were incubated with 25 or 50  $\mu\text{M}$  of inhibitor for 6 h at 37  $^{\circ}\text{C}$  and  $\alpha$ -tubulin acetylation detected by immunofluorescence. (A) At 25  $\mu\text{M}$ , TM, AF8, and AF10 increased  $\alpha$ -tubulin acetylation in HCT116 cells. (B) At 25  $\mu\text{M}$ , C3 did not increase  $\alpha$ -tubulin acetylation, C5 slightly increased  $\alpha$ -tubulin acetylation, and C10 more strongly increased  $\alpha$ -tubulin acetylation. (C) At 50  $\mu\text{M}$ , TM, AF8, and AF10 also increased  $\alpha$ -tubulin acetylation. (D) At 50  $\mu\text{M}$ , C3 did not increase  $\alpha$ -tubulin acetylation, but C5 and C10 increased  $\alpha$ -tubulin acetylation.

consistent with more potent *in vitro* SIRT2 inhibition ( $\text{IC}_{50}$  0.036  $\mu\text{M}$ ) (Figure 4B,D). These observations helped to further validate the results from the *in vitro* sirtuin inhibition assay.

We next tested whether AF8 and AF10 inhibit SIRT1 deacetylase activity in HCT116 cells by monitoring the acetylation of p53, a well-known SIRT1 deacetylation substrate.<sup>31</sup> We also tested compounds C3, C5, and C10 to determine if our *in vitro* SIRT1 inhibition results were consistent with SIRT1 inhibition in cells. HCT116 cells were treated with Trichostatin A, an inhibitor of the zinc-dependent HDACs, and with or without 25  $\mu\text{M}$  of our sirtuin inhibitors. The SIRT1-selective inhibitor EX527 increased p53 acetylation, consistent with previous reports (Figure 5).<sup>25,32</sup> TM, AF8, and AF10 did not increase the levels of acetyl p53, indicating that they inhibit SIRT2 but not SIRT1 in cells. Compound C3 also did not increase the acetylation of p53, consistent with the lack of *in vitro* SIRT1 inhibition ( $\text{IC}_{50}$  > 100  $\mu\text{M}$ ). Inhibitors C5 and C10 moderately increased the acetylation of p53, consistent with the lack of significant SIRT2/SIRT1 selectivity for the compounds (34 and 12-fold respective SIRT2/SIRT1 selectivity). To more closely examine the inhibition of SIRT1 in cells, HCT116 cells were cotreated with trichostatin A and 10–50  $\mu\text{M}$  of AF8, AF10, and C10. Compound C10 demonstrated a dose-dependent increase in acetyl p53 levels, consistent with *in vitro* SIRT1 inhibition ( $\text{IC}_{50}$  0.45  $\mu\text{M}$ ) and lack of significant SIRT2/SIRT1 selectivity (Figure 5). AF8 did not increase acetyl p53 levels

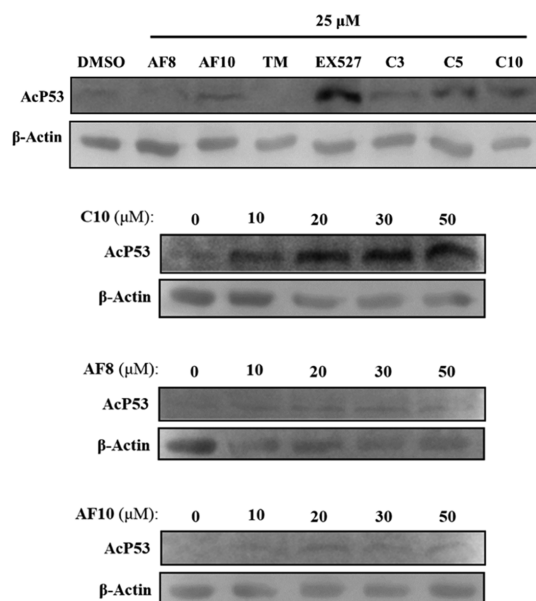


**Figure 5.** AF8 and AF10 did not noticeably increase p53 acetylation. HCT116 cells were co-incubated with 400 nM TSA and 25  $\mu\text{M}$  of TM, AF8, AF10, C3, C5, C10, and EX527 for 6 h and p53 K382 acetylation levels analyzed by western blot. Known SIRT1 inhibitor EX527 dramatically increased acetyl p53 levels, while compounds C5 and C10 moderately increased acetyl p53 levels. A dose-dependent increase of acetyl p53 was observed upon treatment with C10, but not AF8 and AF10.

in a dose-dependent manner, indicating a lack of SIRT1 inhibition. A very slight increase in acetyl p53 was observed with AF10, but there was no correlation between AF10 concentration and acetyl p53 level, indicating a lack of meaningful SIRT1 inhibition (Figure 5). This result suggests that the *in vitro* selectivity of AF8 and AF10 (203 and >1000-fold selectivity, respectively), is sufficient to ensure SIRT2 specific inhibition in cells.

**AF8 and AF10 Significantly Reduced Tumor Growth in a HCT116 Xenograft Mice Model of Colorectal Cancer.** Immunodeficient NOD scid gamma mice (NSG mice) were grafted with HCT116 cells to form tumors and then treated with varying doses of AF8, AF10, or vehicle by intraperitoneal injection over the course of 11 days before the mice were sacrificed and the tumors weighed. As shown in Figure 6A, AF8 at 25 mg/kg slightly decreased tumor growth by volume and weight but did not result in a statistically significant difference. AF8 at 100 mg/kg significantly ( $p < 0.0001$ ) inhibited tumor growth by 80% as measured by the average tumor volume on the last day of treatment. This was consistent with the significant ( $p = 0.0001$ ) difference in average tumor weight that demonstrated an inhibition of 78%. However, AF10 was less potent in this xenograft model. At 100 mg/kg, AF10-inhibited tumor growth significantly ( $p = 0.0114$ ), but only by 37% as measured by the final tumor volume (Figure 6B). This was similar to the significant ( $p = 0.0152$ ) tumor inhibition of 49% as measured by final tumor weight. No significant weight loss was observed in either the AF8 or AF10 treatment groups.

HCT116 xenograft tumor data suggest that thiourea SIRT2 inhibitors present a possible new therapeutic approach for treating colorectal cancers. Targeted therapies for colorectal cancer are generally more limited to antibodies targeting

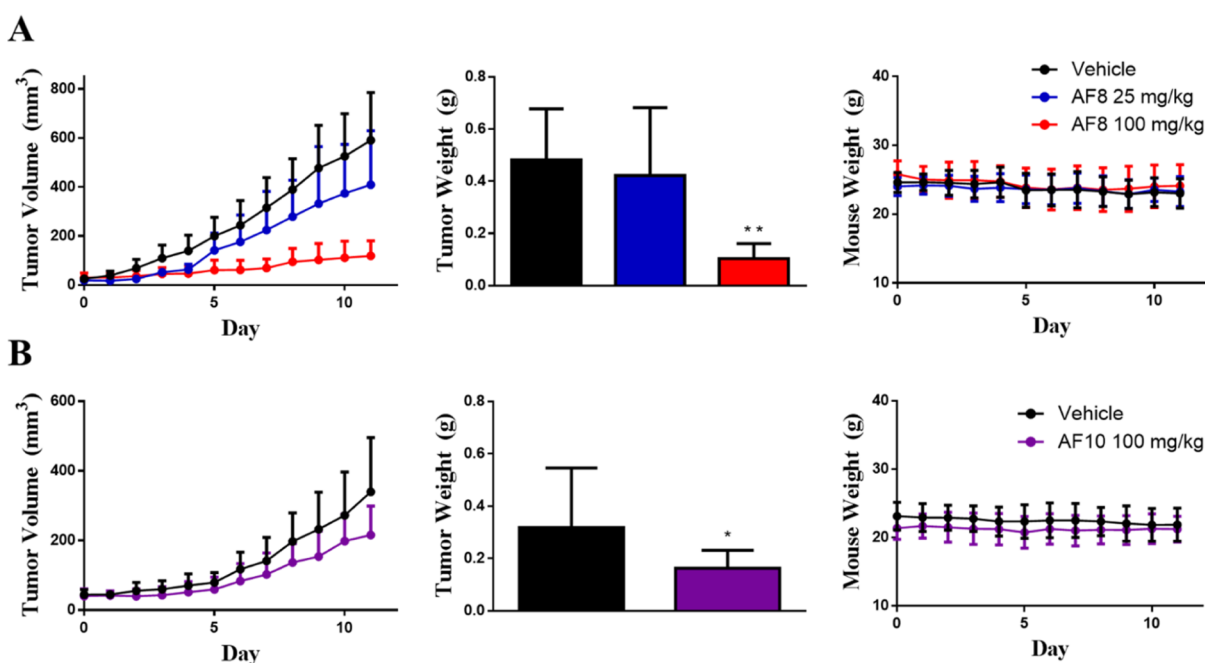


**Figure 6.** AF8 and AF10 significantly inhibit tumor growth by volume and weight in a HCT116 xenograft murine model of colorectal cancer. (A) Tumor volume, tumor weight, and mouse body weight for mice treated with vehicle ( $n = 4$ ), AF8 25 mg/kg ( $n = 3$ ), AF8 100 mg/kg ( $n = 4$ ). (B) Tumor volume, tumor weight, and mouse body weight for mice treated with vehicle ( $n = 6$ ) or AF10 100 mg/kg ( $n = 8$ ). Statistical results were analyzed with an unpaired, two-tailed  $t$ -test. \* indicates  $P$  value  $< 0.05$  and \*\* indicates  $P$  value  $< 0.01$ .

angiogenesis through VEGF/VEGFR and growth through EGFR.<sup>33,34</sup> Such therapies have met moderate success because of the high-mutation load found in colorectal cancer, and are frequently less effective against colorectal cancers with constitutively active KRas mutations.<sup>35–37</sup> The potent inhibition of HCT116 (KRAS<sup>G13D</sup>) xenograft mice tumor growth by AF8 suggests that targeting SIRT2 activity can be a viable therapeutic strategy in colorectal cancers containing a KRAS mutation. Given the broad toxicity of AF8 and AF10 in other cancer cell lines, it is also possible that SIRT2 inhibitors can be useful for treating other type of cancers.

## CONCLUSIONS

We have developed thiourea mechanism-based inhibitors for SIRT2. Among them, AF8–AF12 are highly selective and potent at inhibiting SIRT2 *in vitro*. Compared with the previous thioamide-type inhibitor TM, these thiourea compounds are much easier to synthesize, which allowed us to quickly prepare many compounds. In addition, AF8 is less hydrophobic than TM and thus is more desirable as a therapeutic candidate.

AF8 and AF10 showed cytotoxicity across a variety of breast, lung, pancreatic, and colorectal cancer cell lines, but showed generally less toxicity in normal cells which suggested that cancer cells could have an increased dependence on SIRT2 activity. AF8 and AF10 also inhibited SIRT2, but not SIRT1 in cells. AF8 at 100 mg/kg inhibited tumor growth by 80% in a HCT116 xenograft mouse model. Although in cell culture AF10 is more potent than AF8, in the mouse xenograft model, AF8 is better than AF10. This is likely because other properties, such as solubility (AF8-predicted  $cLogS$  is  $-6.5$ , AF10-predicted  $cLogS$  is  $-7.0$ ), are more important for *in vivo* efficacy, which should be useful for the future development of new SIRT2 inhibitors as anticancer therapeutic candidates. This represents one of the few studies examining the

anticancer effect of SIRT2 inhibition in a mouse xenograft model of tumors. The results further support that SIRT2 inhibition is a promising cancer treatment strategy and that developing new and improved SIRT2 inhibitors is warranted, a task that will be facilitated by the facile synthesis procedure of the thiourea-type of SIRT2 inhibitors.

## EXPERIMENTAL SECTION

**General.** All reagents were purchased from commercial sources and used without further purification. Reactions were checked for completion by LC–MS and compounds purified through flash chromatography (SiliaFlash Silica Gel, P60). The Cornell University NMR Facility was used to obtain NMR spectra. <sup>1</sup>H spectra (500 MHz, chloroform-*d*) and <sup>13</sup>C NMR spectra (126 MHz, chloroform-*d*) were obtained on a Bruker 500 MHz with cryoprobe. High-resolution MS was obtained using either an ESI-Orbitrap mass spectrometer or DART-Orbitrap mass spectrometer. The purity of synthesized compounds was confirmed to be  $\geq 95\%$  purity by qNMR.

**LC–MS System.** Analysis of reaction mixtures and purified compounds was carried out using a Shimadzu HPLC LC20-AD system connected to a Thermo Scientific LCQ Fleet Ion Trap mass spectrometer, Rugged Ion Max Source (electrospray ionization), and reverse phase Phenomenex Kinetex EVO C18 column ( $30 \times 2.1$  mm,  $5 \mu\text{M}$ ). Samples were diluted in water/acetonitrile (1:1) and analyzed using water with 0.1% acetic acid (solvent A) and acetonitrile with 0.1% acetic acid (solvent B) at a constant flow rate of 0.2 mL/min, recording UV absorbance at 215 and 260 nm and positive mode detection of ions.

**General Procedure for the Synthesis of 1a–b as Shown through the Preparation of Benzyl tert-Butyl (6-((3-Hydroxyphenyl)amino)-6-oxohexane-1,5-diyl)(S)-dicarbamate (1a).** Cbz-L-Lys(Boc)-OH (3 g, 7.89 mmol, 1 equiv) was dissolved in dichloromethane (48 mL). To this solution, *N*-methylmorpholine (1.39 mL, 12.6 mmol, 1.6 equiv) and isobutyl chloroformate (1.43 mL, 11.0 mmol, 1.4 equiv) were sequentially added and the reaction mixture stirred for 1 h at room temperature (RT). Then, 3-aminophenol (1.022 g, 9.45 mmol, 1.2 equiv) (or aniline for 1b) was added and the reaction mixture stirred for 16 h at RT. The reaction was checked for completion by

thin-layer chromatography (hexanes/ethyl acetate 1:1) and LC–MS. The reaction mixture was further diluted in dichloromethane (75 mL) and sequentially washed with water (3 × 75 mL) and saturated brine (1 × 75 mL). The organic layer was collected, dried over Na<sub>2</sub>SO<sub>4</sub>, and concentrated by rotary evaporation to yield a viscous, yellow oil. The crude product was purified by silica gel column chromatography (hexanes/ethyl acetate 1:1) to yield **1a** as a pale yellow solid in 80% yield (2.98 g). <sup>1</sup>H NMR (500 MHz, chloroform-*d*): δ 8.74 (d, *J* = 31.9 Hz, 1H), 7.45 (s, 1H), 7.41–7.30 (m, 5H), 7.20–7.08 (m, 1H), 6.87 (s, 1H), 6.64 (dd, *J* = 8.1, 2.3 Hz, 1H), 5.93 (d, *J* = 23.4 Hz, 1H), 5.18–5.02 (m, 2H), 4.75 (s, 1H), 4.37 (d, *J* = 8.4 Hz, 1H), 3.08 (d, *J* = 7.0 Hz, 2H), 1.90 (d, *J* = 13.6 Hz, 1H), 1.82–1.64 (m, 1H), 1.56–1.32 (m, 13H). <sup>13</sup>C NMR (126 MHz, chloroform-*d*): δ 170.9, 157.0, 156.9, 156.6, 138.5, 135.9, 129.9, 128.6, 128.3, 128.2, 112.0, 111.6, 107.4, 79.7, 67.4, 55.9, 39.7, 31.6, 29.5, 28.4, 22.5. HRMS [DART-Orbitrap] *m/z*: calcd for C<sub>24</sub>H<sub>34</sub>N<sub>3</sub>O<sub>4</sub> ([M – CO<sub>2</sub> + H]<sup>+</sup>), 428.2544; observed, 428.2567.

**Benzyl tert-Butyl (6-oxo-6-(Phenylamino)hexane-1,5-diyl)(S)-dicarbamate (1b)**. White, powdery solid. 94% yield. <sup>1</sup>H NMR (500 MHz, chloroform-*d*): δ 8.46 (d, *J* = 47.9 Hz, 1H), 7.53 (d, *J* = 7.9 Hz, 2H), 7.44–7.29 (m, 7H), 7.17–7.08 (m, 1H), 5.71 (d, *J* = 28.3 Hz, 1H), 5.13 (d, *J* = 3.2 Hz, 2H), 4.69 (s, 1H), 4.33 (s, 1H), 3.11 (s, 2H), 2.07–1.88 (m, 1H), 1.75 (dtd, *J* = 14.1, 8.6, 5.4 Hz, 1H), 1.44 (s, 14H). <sup>13</sup>C NMR (126 MHz, chloroform-*d*): δ 170.2, 156.7, 156.4, 137.7, 136.1, 128.9 (d, *J* = 1.2 Hz), 128.6, 128.3 (d, *J* = 1.4 Hz), 128.1 (d, *J* = 2.7 Hz), 124.4, 120.0 (d, *J* = 2.4 Hz), 79.4, 67.3, 55.6, 39.5, 31.6, 29.5, 28.4, 22.5, 19.1. HRMS [DART-Orbitrap] *m/z*: calcd for C<sub>24</sub>H<sub>34</sub>N<sub>3</sub>O<sub>3</sub> ([M – CO<sub>2</sub> + H]<sup>+</sup>), 412.2595; observed, 412.2618.

**General Procedure for 2a–b Synthesis as Shown through the Preparation of Benzyl (S)-(1-(3-Hydroxyphenyl)amino)-6-isothiocyanato-1-oxohexan-2-yl)carbamate (2a)**. Compound **1a** (1 g, 2.12 mmol, 1 equiv) was dissolved in dichloromethane (14 mL) and trifluoroacetic acid (7 mL). Reaction was stirred for 1 h at RT before being concentrated by rotary evaporation to remove the trifluoroacetic acid. The crude mixture was dissolved in tetrahydrofuran (21 mL) before 1,1'-thiocarbonyl diimidazole (454 mg, 2.54 mmol, 1.2 equiv) and triethylamine (TEA, 0.73 mL, 5.3 mmol, 2.5 equiv) were sequentially added. The reaction was stirred for 16 h at RT and then further diluted in ethyl acetate (100 mL) and washed with water (3 × 60 mL) and saturated brine (1 × 60 mL). The organic layer was collected, dried over Na<sub>2</sub>SO<sub>4</sub>, and concentrated by rotary evaporation. The crude product was purified by flash chromatography (hexanes/ethyl acetate 2:1) to afford **2a** as a white solid in 68% yield (594 mg). <sup>1</sup>H NMR (500 MHz, chloroform-*d*): δ 8.55 (s, 1H), 7.46 (s, 1H), 7.35 (d, *J* = 3.0 Hz, 5H), 7.14 (t, *J* = 8.1 Hz, 1H), 6.79 (d, *J* = 7.9 Hz, 1H), 6.64 (dd, *J* = 8.2, 2.3 Hz, 1H), 5.65 (d, *J* = 7.2 Hz, 1H), 5.15 (q, *J* = 12.2 Hz, 2H), 4.37 (d, *J* = 8.2 Hz, 1H), 3.56–3.35 (m, *J* = 6.9, 6.4 Hz, 2H), 2.01–1.84 (m, 1H), 1.70 (tdd, *J* = 22.8, 11.4, 6.1 Hz, 2H), 1.61–1.35 (m, 2H). <sup>13</sup>C NMR (126 MHz, chloroform-*d*): δ 170.5, 156.8, 138.2, 135.7, 130.2, 130.0, 128.6, 128.4, 128.1, 112.2, 111.6, 107.4, 67.7, 55.7, 44.7, 31.4, 29.4, 22.8. HRMS [DART-Orbitrap] *m/z*: calcd for C<sub>21</sub>H<sub>24</sub>N<sub>3</sub>O<sub>4</sub>S ([M + H]<sup>+</sup>), 414.1482; observed, 414.1507.

**Benzyl (S)-(6-Isothiocyano-1-oxo-1-(phenylamino)hexan-2-yl)carbamate (2b)**. White solid, 86% yield. <sup>1</sup>H NMR (500 MHz, chloroform-*d*): δ 8.37 (s, 1H), 7.49 (d, *J* = 7.9 Hz, 2H), 7.42–7.25 (m, 7H), 7.13 (t, *J* = 7.4 Hz, 1H), 5.60 (d, *J* = 8.8 Hz, 1H), 5.14 (q, *J* = 12.2 Hz, 2H), 4.38 (q, *J* = 7.9, 7.3 Hz, 1H), 3.62–3.40 (m, *J* = 7.0, 6.2 Hz, 2H), 1.98 (ddt, *J* = 13.7, 10.1, 6.1 Hz, 1H), 1.87–1.63 (m, 4H), 1.55 (tdd, *J* = 16.2, 11.6, 7.0 Hz, 2H). <sup>13</sup>C NMR (126 MHz, chloroform-*d*): δ 169.8, 156.7, 137.4, 135.9, 130.4, 129.0, 128.6, 128.4, 128.1, 124.7, 120.1, 67.5, 55.4, 44.8, 31.5, 29.5, 22.7. HRMS [DART-Orbitrap] *m/z*: calcd for C<sub>21</sub>H<sub>24</sub>N<sub>3</sub>O<sub>3</sub>S ([M + H]<sup>+</sup>), 398.1533; observed, 398.1556.

**Benzyl (S)-(6-(3-Hexylthioureido)-1-oxo-1-(phenylamino)hexan-2-yl)carbamate (AF6)**. White solid, 80% yield. <sup>1</sup>H NMR (500 MHz, chloroform-*d*): δ 8.56 (s, 1H), 7.54 (d, *J* = 7.9 Hz, 2H), 7.41–7.23 (m, 7H), 7.15–7.08 (m, 1H), 6.09 (s, 2H), 5.76 (d, *J* = 7.8 Hz, 1H), 5.20–5.03 (m, 2H), 4.39 (t, *J* = 7.5 Hz, 1H), 3.42 (d, *J* = 68.8 Hz, 4H), 1.94 (dt, *J* = 14.5, 7.6 Hz, 1H), 1.83–1.71 (m, 1H), 1.64 (d, *J* = 7.6 Hz, 2H), 1.50 (dq, *J* = 38.3, 6.9 Hz, 4H), 1.37–1.14 (m, 7H),

0.98–0.72 (m, 3H). <sup>13</sup>C NMR (126 MHz, chloroform-*d*): δ 181.3, 170.2, 156.7, 137.5, 136.0, 129.0, 128.6, 128.3, 128.0, 124.7, 120.1, 67.3, 55.3, 43.8, 31.8, 31.4, 29.7, 28.9, 28.2, 26.6, 22.5 (d, *J* = 3.3 Hz), 14.0. HRMS [DART-Orbitrap] *m/z*: calcd for C<sub>27</sub>H<sub>39</sub>N<sub>4</sub>O<sub>3</sub>S ([M + H]<sup>+</sup>), 499.2737; observed, 499.2766.

**Benzyl (S)-(6-(3-Heptylthioureido)-1-oxo-1-(phenylamino)hexan-2-yl)carbamate (AF7)**. White solid, 85% yield. <sup>1</sup>H NMR (500 MHz, chloroform-*d*): δ 8.51 (s, 1H), 7.54 (d, *J* = 8.0 Hz, 2H), 7.41–7.27 (m, 7H), 7.17–7.08 (m, 1H), 6.08 (s, 2H), 5.71 (d, *J* = 8.0 Hz, 1H), 5.13 (d, *J* = 5.2 Hz, 2H), 4.39 (d, *J* = 8.0 Hz, 1H), 3.43 (d, *J* = 71.3 Hz, 3H), 1.96 (dt, *J* = 14.1, 7.5 Hz, 1H), 1.76 (dtd, *J* = 13.9, 8.6, 5.8 Hz, 1H), 1.72–1.60 (m, 2H), 1.60–1.37 (m, 4H), 1.37–1.12 (m, 9H), 0.94–0.82 (m, 3H). <sup>13</sup>C NMR (126 MHz, chloroform-*d*): δ 181.1, 170.2, 156.7, 137.5, 136.0, 129.0, 128.6, 128.3, 128.0, 124.6, 120.1, 67.3, 55.2, 43.8, 31.8, 31.7, 28.9, 28.3–28.0 (m), 26.9, 22.6, 22.5, 14.1 (d, *J* = 3.0 Hz). HRMS [DART-Orbitrap] *m/z*: calcd for C<sub>28</sub>H<sub>41</sub>N<sub>4</sub>O<sub>3</sub>S ([M + H]<sup>+</sup>), 513.2894; observed, 513.2930.

**General Procedure for C1–C12 and AF6–AF12 Synthesis as Shown through the Preparation of Benzyl (S)-(6-(3-Octylthioureido)-1-oxo-1-(phenylamino)hexan-2-yl)carbamate (AF8)**. Compound **2b** (250 mg, 0.63 mmol, 1 equiv) (or **2a** for C1–C12) was dissolved in dimethylformamide (4.2 mL). To this mixture, octylamine (0.26 mL, 1.57 mmol, 2.5 equiv) and triethylamine (0.17 mL, 1.25 mmol, 2 equiv) were sequentially added and the reaction was stirred for 16 h at RT. The reaction mixture was diluted in dichloromethane (50 mL) and washed with water (3 × 25 mL) and saturated brine (1 × 25 mL) before being dried over Na<sub>2</sub>SO<sub>4</sub> and concentrated by rotary evaporation. The crude mixture was purified by flash chromatography (hexanes: ethyl acetate 2:1) to afford **AF8** as a white, crystalline solid in 74% yield (247 mg). <sup>1</sup>H NMR (500 MHz, chloroform-*d*): δ 8.51 (s, 1H), 7.54 (d, *J* = 8.0 Hz, 2H), 7.43–7.24 (m, 7H), 7.17–7.08 (m, 1H), 6.08 (s, 2H), 5.72 (d, *J* = 8.1 Hz, 1H), 5.22–5.02 (m, 2H), 4.39 (d, *J* = 8.5 Hz, 1H), 3.35 (s, 2H), 2.03–1.85 (m, *J* = 6.8 Hz, 1H), 1.76 (dtd, *J* = 13.9, 8.6, 5.7 Hz, 1H), 1.66 (h, *J* = 6.5 Hz, 2H), 1.51 (dq, *J* = 36.6, 7.0 Hz, 4H), 1.37–1.12 (m, 11H), 0.90 (t, *J* = 7.0 Hz, 3H). <sup>13</sup>C NMR (126 MHz, chloroform-*d*): δ 181.0, 170.2, 156.7, 137.5, 136.0, 129.0, 128.6, 128.3, 128.0, 124.6, 120.1, 67.3, 55.2, 43.8, 31.8, 29.24, 29.17, 29.0, 28.2, 26.9, 22.6, 22.5, 14.1. HRMS [DART-Orbitrap] *m/z*: calcd for C<sub>29</sub>H<sub>43</sub>N<sub>4</sub>O<sub>3</sub>S ([M + H]<sup>+</sup>), 527.3050; observed, 527.3078.

**Benzyl (S)-(6-(3-Decylthioureido)-1-oxo-1-(phenylamino)hexan-2-yl)carbamate (AF10)**. White solid, 70% yield. <sup>1</sup>H NMR (500 MHz, chloroform-*d*): δ 8.51 (s, 1H), 7.54 (d, *J* = 7.9 Hz, 2H), 7.42–7.24 (m, 7H), 7.18–7.08 (m, 1H), 6.08 (s, 2H), 5.72 (d, *J* = 8.1 Hz, 1H), 5.22–5.04 (m, 2H), 4.39 (d, *J* = 7.9 Hz, 1H), 3.42 (d, *J* = 76.0 Hz, 4H), 1.95 (dt, *J* = 14.2, 7.5 Hz, 1H), 1.84–1.71 (m, 1H), 1.55 (dddq, *J* = 44.3, 37.4, 14.7, 7.4, 6.9 Hz, 5H), 1.36–1.14 (m, 16H), 0.90 (t, *J* = 6.9 Hz, 3H). <sup>13</sup>C NMR (126 MHz, chloroform-*d*): δ 181.0, 170.2, 156.7, 137.5, 136.0, 129.0, 128.6, 128.3, 128.0, 124.6, 120.1, 67.3, 55.2, 44.3, 43.8, 31.9, 31.8, 29.5 (d, *J* = 2.4 Hz), 29.3 (d, *J* = 1.9 Hz), 29.0, 28.2, 26.9, 22.7, 22.5, 14.1. HRMS [DART-Orbitrap] *m/z*: calcd for C<sub>31</sub>H<sub>47</sub>N<sub>4</sub>O<sub>3</sub>S ([M + H]<sup>+</sup>), 555.3363; observed, 555.3394.

**Benzyl (S)-(6-(3-Dodecylthioureido)-1-oxo-1-(phenylamino)hexan-2-yl)carbamate (AF12)**. White solid, 57% yield. <sup>1</sup>H NMR (500 MHz, chloroform-*d*): δ 8.48 (s, 1H), 7.54 (d, *J* = 8.0 Hz, 2H), 7.43–7.24 (m, 7H), 7.17–7.08 (m, 1H), 6.07 (s, 2H), 5.69 (d, *J* = 8.1 Hz, 1H), 5.14 (d, *J* = 4.5 Hz, 2H), 4.38 (d, *J* = 7.9 Hz, 1H), 3.72–3.21 (m, 2H), 2.04–1.88 (m, 1H), 1.85–1.72 (m, 1H), 1.67 (h, *J* = 6.7 Hz, 1H), 1.60–1.39 (m, 4H), 1.37–1.13 (m, 20H), 0.94–0.86 (m, 3H). <sup>13</sup>C NMR (126 MHz, chloroform-*d*): δ 181.1, 170.1, 156.7, 137.5, 136.0, 129.0, 128.6, 128.3, 128.0, 124.6, 120.1, 67.4, 55.2, 43.8, 31.9, 31.7, 29.7, 29.64, 29.59, 29.53, 29.4, 29.3, 29.0, 28.2, 28.0, 26.9, 22.7, 22.4, 19.1, 14.1. HRMS [DART-Orbitrap] *m/z*: calcd for C<sub>33</sub>H<sub>51</sub>N<sub>4</sub>O<sub>3</sub>S ([M + H]<sup>+</sup>), 583.3676; observed, 583.3704.

**Benzyl (S)-(1-(3-Hydroxyphenyl)amino)-6-(3-methylthioureido)-1-oxohexan-2-yl)carbamate (C1)**. White solid, 48% yield. <sup>1</sup>H NMR (500 MHz, DMSO-*d*<sub>6</sub>): δ 9.87 (s, 1H), 9.37 (s, 1H), 7.53 (d, *J* = 7.9 Hz, 1H), 7.47–7.28 (m, 5H), 7.23–7.14 (m, 1H), 7.07 (t, *J* = 8.0 Hz, 1H), 6.99–6.93 (m, 1H), 6.45 (dd, *J* = 8.0, 2.3 Hz, 1H), 5.04 (s, 2H), 4.11 (td, *J* = 8.5, 5.2 Hz, 1H), 3.33 (s, 7H), 2.79 (s, 3H), 1.73–1.55

(m, 2H), 1.55–1.21 (m, 3H).  $^{13}\text{C}$  NMR (126 MHz, DMSO- $d_6$ ):  $\delta$  171.4, 158.0, 156.5, 140.4, 137.5, 129.8, 129.4, 128.8, 128.7, 128.3, 128.2, 110.8, 110.4, 106.8, 65.9, 55.9, 32.1, 29.0, 23.6. HRMS [ESI-Orbitrap]  $m/z$ : calcd for  $\text{C}_{22}\text{H}_{29}\text{N}_4\text{O}_4\text{S}$  ( $[\text{M} + \text{H}]^+$ ), 445.1904; observed, 445.1908.

**Benzyl (S)-1-((3-Hydroxyphenyl)amino)-1-oxo-6-(3-propylthioureido)hexan-2-yl)carbamate (C3).** White solid, 41% yield.  $^1\text{H}$  NMR (500 MHz, chloroform- $d$ ):  $\delta$  8.82 (s, 1H), 7.47 (s, 2H), 7.40 (t,  $J = 2.2$  Hz, 1H), 7.33 (s, 4H), 7.13 (t,  $J = 8.1$  Hz, 1H), 6.93 (d,  $J = 8.0$  Hz, 1H), 6.65 (dd,  $J = 8.1, 2.3$  Hz, 1H), 6.12 (d,  $J = 50.5$  Hz, 1H), 5.89 (d,  $J = 8.0$  Hz, 1H), 5.22–5.00 (m, 2H), 4.42 (d,  $J = 7.7$  Hz, 1H), 3.36 (d,  $J = 19.1$  Hz, 3H), 1.86 (s, 1H), 1.70 (s, 5H), 1.56 (h,  $J = 7.3$  Hz, 4H), 1.47–1.22 (m, 1H), 0.92 (t,  $J = 7.4$  Hz, 3H).  $^{13}\text{C}$  NMR (126 MHz, chloroform- $d$ ):  $\delta$  181.2, 171.0, 156.9, 138.3, 135.8, 130.0, 128.6, 128.4, 128.1, 112.3, 112.0, 107.6, 67.5, 55.6, 43.6, 31.9, 29.7, 28.3, 22.6, 22.3, 11.4. HRMS [ESI-Orbitrap]  $m/z$ : calcd for  $\text{C}_{24}\text{H}_{33}\text{N}_4\text{O}_4\text{S}$  ( $[\text{M} + \text{H}]^+$ ), 473.2217; observed, 473.2222.

**Benzyl (S)-1-((3-Hydroxyphenyl)amino)-1-oxo-6-(3-pentylthioureido)hexan-2-yl)carbamate (C5).** White solid, 94% yield.  $^1\text{H}$  NMR (500 MHz, DMSO- $d_6$ ):  $\delta$  9.87 (s, 1H), 9.37 (s, 1H), 7.53 (d,  $J = 7.9$  Hz, 1H), 7.37 (d,  $J = 5.4$  Hz, 4H), 7.35–7.25 (m, 2H), 7.19 (q,  $J = 2.8, 2.2$  Hz, 1H), 7.07 (t,  $J = 8.1$  Hz, 1H), 6.99–6.93 (m, 1H), 6.45 (dd,  $J = 8.1, 2.3$  Hz, 1H), 5.04 (s, 2H), 4.11 (td,  $J = 8.6, 5.3$  Hz, 1H), 3.33 (s, 10H), 1.63 (ddd,  $J = 18.2, 9.4, 4.4$  Hz, 1H), 1.45 (p,  $J = 7.2$  Hz, 3H), 1.41–1.16 (m, 5H), 0.87 (t,  $J = 7.1$  Hz, 3H).  $^{13}\text{C}$  NMR (126 MHz, DMSO- $d_6$ ):  $\delta$  171.4, 158.0, 156.5, 140.4, 137.5, 129.8, 128.8, 128.3, 128.2, 110.8, 110.4, 106.8, 65.9, 55.9, 32.1, 29.1, 28.9, 23.6, 22.4, 14.4. HRMS [ESI-Orbitrap]  $m/z$ : calcd for  $\text{C}_{26}\text{H}_{37}\text{N}_4\text{O}_4\text{S}$  ( $[\text{M} + \text{H}]^+$ ), 501.2530; observed, 501.2532.

**Benzyl (S)-1-((3-Hydroxyphenyl)amino)-6-(3-octylthioureido)-1-oxohexan-2-yl)carbamate (C8).** White solid, 79% yield.  $^1\text{H}$  NMR (500 MHz, chloroform- $d$ ):  $\delta$  9.07 (s, 1H), 8.18 (s, 1H), 7.39 (s, 1H), 7.29 (p,  $J = 6.8, 5.7$  Hz, 5H), 7.05 (t,  $J = 8.0$  Hz, 1H), 6.89 (d,  $J = 8.0$  Hz, 1H), 6.71–6.55 (m, 1H), 6.55–6.19 (m, 2H), 6.14 (d,  $J = 7.9$  Hz, 1H), 5.21–4.87 (m, 2H), 4.39 (q,  $J = 7.3$  Hz, 1H), 3.71–2.98 (m, 4H), 2.58 (s, 1H), 1.78 (d,  $J = 12.0$  Hz, 1H), 1.71–1.57 (m, 1H), 1.48 (dt,  $J = 19.7, 8.5$  Hz, 3H), 1.39–1.04 (m, 14H), 0.88 (t,  $J = 7.0$  Hz, 3H).  $^{13}\text{C}$  NMR (126 MHz, chloroform- $d$ ):  $\delta$  180.9, 171.4, 156.9, 138.3, 135.8, 129.9, 128.6, 128.3, 128.0, 112.3, 112.0, 107.8, 67.4, 55.7, 44.2 (d,  $J = 89.0$  Hz), 32.0, 31.8, 29.7, 29.3, 29.2, 29.1, 28.3, 26.9, 22.7, 22.6, 14.1. HRMS [ESI-Orbitrap]  $m/z$ : calcd for  $\text{C}_{29}\text{H}_{43}\text{N}_4\text{O}_4\text{S}$  ( $[\text{M} + \text{H}]^+$ ), 543.3000; observed, 543.3004.

**Benzyl (S)-6-(3-Decylthioureido)-1-((3-Hydroxyphenyl)amino)-1-oxohexan-2-yl)carbamate (C10).** White solid, 80% yield.  $^1\text{H}$  NMR (500 MHz, chloroform- $d$ ):  $\delta$  9.04 (s, 1H), 8.09 (s, 1H), 7.39 (s, 1H), 7.29 (s, 5H), 7.06 (t,  $J = 8.1$  Hz, 1H), 6.90 (d,  $J = 8.0$  Hz, 1H), 6.68–6.54 (m, 1H), 6.29 (d,  $J = 69.3$  Hz, 2H), 6.10 (d,  $J = 7.9$  Hz, 1H), 5.21–4.88 (m, 2H), 4.40 (q,  $J = 7.4$  Hz, 1H), 3.60–3.01 (m, 4H), 2.42 (s, 1H), 1.78 (s, 1H), 1.71–1.57 (m, 1H), 1.49 (dt,  $J = 21.7, 7.2$  Hz, 4H), 1.26 (d,  $J = 5.6$  Hz, 15H), 0.89 (t,  $J = 7.0$  Hz, 3H).  $^{13}\text{C}$  NMR (126 MHz, chloroform- $d$ ):  $\delta$  180.9, 171.4, 156.9, 138.3, 135.8, 130.0, 128.6, 128.3, 128.0, 112.3, 112.0, 107.8, 67.4, 55.7, 44.2 (d,  $J = 82.2$  Hz), 32.0, 31.9, 29.6, 29.4, 29.3, 29.1, 28.4, 27.0, 22.8, 22.7, 14.1. HRMS [ESI-Orbitrap]  $m/z$ : calcd for  $\text{C}_{31}\text{H}_{47}\text{N}_4\text{O}_4\text{S}$  ( $[\text{M} + \text{H}]^+$ ), 571.3313; observed, 571.3311.

**Benzyl (S)-6-(3-dodecylthioureido)-1-((3-Hydroxyphenyl)amino)-1-oxohexan-2-yl)carbamate (C12).** White solid, 82% yield.  $^1\text{H}$  NMR (500 MHz, chloroform- $d$ ):  $\delta$  9.01 (s, 1H), 8.00 (d,  $J = 8.0$  Hz, 1H), 7.39 (s, 1H), 7.30 (s, 5H), 7.08 (t,  $J = 8.1$  Hz, 1H), 6.91 (d,  $J = 8.0$  Hz, 1H), 6.62 (dd,  $J = 8.0, 2.2$  Hz, 1H), 6.54–6.10 (m, 2H), 6.06 (d,  $J = 7.9$  Hz, 1H), 5.20–4.92 (m, 2H), 4.40 (q,  $J = 7.4$  Hz, 1H), 3.66–3.01 (m, 4H), 2.20 (s, 1H), 1.98–1.72 (m, 1H), 1.66 (d,  $J = 11.1$  Hz, 1H), 1.50 (dt,  $J = 16.3, 7.7$  Hz, 4H), 1.42–1.06 (m, 20H), 0.90 (t,  $J = 6.9$  Hz, 3H).  $^{13}\text{C}$  NMR (126 MHz, chloroform- $d$ ):  $\delta$  181.0, 171.3, 156.9, 138.3, 135.8, 130.0, 128.6, 128.3, 128.0, 112.3, 112.0, 107.7, 67.5, 55.7, 44.2 (d,  $J = 103.5$  Hz), 32.0, 31.9, 29.69, 29.67, 29.64, 29.59, 29.4 (d,  $J = 1.4$  Hz), 29.1, 28.3, 27.0, 22.7, 14.2. HRMS [ESI-Orbitrap]  $m/z$ : calcd for  $\text{C}_{33}\text{H}_{51}\text{N}_4\text{O}_4\text{S}$  ( $[\text{M} + \text{H}]^+$ ), 599.3626; observed, 599.3625.

**Sirtuin Purification.** Human SIRT1–3 were all expressed and purified as previously reported.<sup>10</sup>

**Enzyme IC<sub>50</sub> Assay.** Inhibitors were stored at  $-20$  °C as stock solutions in DMSO (20–50 mM) and further serial dilutions were prepared on the day of the assay. Inhibitors were tested in duplicate at final concentrations ranging from 0.002 to 417  $\mu\text{M}$  with DMSO as control. At 0 °C, sirtuins were diluted in the reaction buffer (20 mM Tris, 1 mM NAD<sup>+</sup>, 1 mM dithiothreitol, pH 8.0) to the final concentration (0.05  $\mu\text{M}$  SIRT1, 0.2  $\mu\text{M}$  SIRT2, 0.05  $\mu\text{M}$  SIRT3). Inhibitors were added to the appropriate SIRT1–3 reaction mixture and preincubated at 37 °C for 15 min. Acetyl H3K9 peptide (10  $\mu\text{M}$  final concentration) was added to start the reaction, and the reaction mixture further incubated at 37 °C until 10–18% of the peptide was deacetylated (3 min for SIRT1, 6 min for SIRT2, and 15 min for SIRT3). The reaction was quenched by the addition of aqueous acid (0.2 M HCl, 6 M acetic acid) at an equal volume, followed by vigorous vortexing. Samples were then centrifuged at 17 000g for 2 min at RT to pellet the enzyme. The supernatant was then analyzed by analytical HPLC on a Shimadzu LC, Phenomenex Kinetex EVO C18 column (100  $\times$  4.60 mm, 5  $\mu\text{M}$ , 100 Å), UV absorbance measurement at 215 and 326 nm, 0.1% trifluoroacetic acid in water (solvent A), 0.1% trifluoroacetic acid in acetonitrile (solvent B), and 0.5 mL/min flow rate. The peak areas of deacetylated to acetylated H3K9 peptide were used to quantify deacetylase activity. Deacetylase activity was then normalized to the DMSO control, and log(inhibitor concentration) versus normalized deacetylase activity fitted by nonlinear regression to  $Y = 100/(1 + 10^{(X - \log \text{IC}_{50})})$  on GraphPad Prism version 6.01.

**Cell Cytotoxicity Assay.** To a flat bottom 96-well plate, 1000–3000 cells were seeded into each well and incubated for 20 h at 37 °C (1000 cells for HCT-116, 2000 cells for MDA-MB-231, MDA-MB-468, NCI-H23, A549, SW948 and 3000 cells for MCF7, BxPC-3, CCD 841 CoN, and HME1). Inhibitors in varying final concentrations (1–100  $\mu\text{M}$ ) were added to each well and the cells incubated for 72 h at 37 °C. Then, 100  $\mu\text{L}$  of media was removed from each well and 20  $\mu\text{L}$  of CellTiter-Blue (Promega) was added to each well. The 96-well plate was then incubated for 4 h at 37 °C to measure cell viability. The fluorescence of each well (560 nm excitation/590 nm emission) was measured using a Fluoroskan Ascent FL microplate fluorometer. The fluorescence was normalized to DMSO-treated cells, and GraphPad Prism software used to plot the cell viability curves and calculate the GI<sub>50</sub> value for each cell line.

**Soft Agar Assay.** HCT116 cells in a 10 cm dish (70–80% confluent) were rinsed with phosphate-buffered saline (PBS), trypsinized for 1 min, resuspended in media (McCoy's medium +10% calf serum), and counted by hemocytometry. To make the solid base layer, a stock 3% agar solution in water was heated to 42 °C, diluted to 0.6% in media, and mixed with inhibitors to final concentrations of 2.5–50  $\mu\text{M}$ . To each well in a six-well plate, 2 mL of the base layer was added and allowed to solidify for 1 h at room temperature. To make the growth layer, the stock 3% agar solution was diluted to 0.3% in media and inhibitors were added to final concentrations of 2.5–50  $\mu\text{M}$ . Then, HCT116 cells were added to the growth layer to a concentration of 500 cells/mL. In triplicate, 2 mL of the growth layer-containing inhibitor and HCT116 cells was added to each well and incubated at 37 °C. After five days, another 2 mL of growth layer-containing inhibitor was added to each well. After 9–11 days, 200  $\mu\text{L}$  of nitro blue tetrazolium chloride in water (2 mg/mL) was added to each well and incubated overnight at 37 °C. The plates were imaged using a ChemiDoc MP Imaging System and colonies were counted with ImageJ software.

**Xenograft Mice Study.** All animals used in this study were handled in accordance with federal and institutional guidelines, under a protocol approved by the Cornell University Institutional Animal Care and Use Committee. Immunodeficient female and male NSG mice were purchased from The Jackson Laboratory. When mice were approximately four to eight weeks old,  $1 \times 10^6$  HCT116 cells were injected on both sides of the abdomen. The cells were allowed to grow for 3–5 days until the tumors were just large enough to be visible and measured. Inhibitors were dissolved in solution (80% PBS,

10% DMSO, 10% Kolliphor EL) to a concentration of 10 mg/mL before injection into mice. AF8 at 25 mg/kg ( $n = 3$ ) and 100 mg/kg ( $n = 4$ ), or vehicle ( $n = 4$ ), was intraperitoneally injected every day over the course of 12 days. AF10 at 100 mg/kg ( $n = 8$ ) or vehicle ( $n = 6$ ) was also intraperitoneally injected every day over the course of 12 days. Tumor volume was measured daily and mice were sacrificed on the last day and the tumors extracted and weighed.

**Immunofluorescence Microscopy.** 400 000 HCT116 cells were seeded per dish (MatTek 35 mm, no. 1.5 coverslip, 14 mm glass diameter, poly-D-lysine coated) and incubated for 24 h at 37 °C. Each well was then treated with DMSO or inhibitor at a final concentration of 50  $\mu$ M and incubated for 6 h at 37 °C. Cells were fixed in ice cold methanol for 10 min and rinsed 3 $\times$  in detergent containing buffer (Tris-buffered saline or TBS, 0.1% TX-100). Cells were blocked in blocking buffer (TBS, 0.1% TX-100, 5% BSA) for 1 h at RT and then incubated in primary acetyl  $\alpha$ -tubulin antibody (Millipore MABT868 1:100 dilution) overnight at 4 °C. Cells were then washed 3 $\times$  in detergent containing buffer and incubated with secondary antibody (Cy3-conjugated goat  $\alpha$ -mouse, Thermo Fisher A10521, 1:500 dilution) for 1 h at RT. Cells were rinsed 5 $\times$  in detergent containing buffer and mounted overnight at RT (DAPI Fluoromount-G, SouthernBiotech). Cells were imaged using a Zeiss LSM880 inverse laser scanning confocal microscope.

**P53 Acetylation Assay and Western Blotting.** 400 000 HCT116 cells were seeded per well in a six-well plate and incubated for 24 h at 37 °C. Subsequently, each well was cotreated with 400 nM TSA and respective concentration of AF8, AF10, TM, EX527, C3, C5, or C10 for 6 h at 37 °C before cells were collected and lysed in buffer [4% sodium dodecyl sulfate (SDS), 150 mM NaCl, 50 mM triethanolamine, Universal Nuclease, pH 7.4]. The protein concentrations of cell lysates were calculated using the BCA assay. To evaluate AcP53 (K382) levels, 50  $\mu$ g of lysate was run on a 12% SDS-polyacrylamide gel electrophoresis gel. To check protein loading, 8  $\mu$ g of lysate was also loaded on the same gel. The protein gel was transferred to a polyvinylidene difluoride membrane, blocked in buffer (TBS, 5% BSA, 0.1% Tween-20) for 1 h at RT, and incubated overnight at 4 °C with AcP53 (K382) antibody (CST 2525S), or with  $\beta$ -actin antibody (SCBT sc-47778) for 1 h at RT. Membranes were rinsed with TBST (5 $\times$ , 7 min each) and incubated with antirabbit or antimouse secondary antibody (CST 7074S and CST 7076S) for 1 h at RT. Membranes were rinsed again with TBST (5 $\times$ , 7 min each) before being incubated with ECL substrate and imaged on a Typhoon FLA 7000.

**Cell Culture.** Cell lines were cultured in Dulbecco's modified Eagle medium with 10% fetal bovine serum (FBS; MCF-7, 293T, MDA-MB-231, MDA-MB-468, HME1, CCD 841 CoN), RPMI with 10% FBS (A549, SW948, NCIH23, BxPC-3), McCoy's media with 10% calf serum (HCT116). Cells were incubated at 37 °C with 5% CO<sub>2</sub>.

## ■ ASSOCIATED CONTENT

### ● Supporting Information

The Supporting Information is available free of charge on the ACS Publications website at DOI: 10.1021/acs.jmedchem.9b00191.

In vitro inhibition assays of SIRT1-3 with compounds AF8–AF12, cell cytotoxicity assay of various cell lines comparing compounds AF8, AF10, and TM, and <sup>1</sup>H and <sup>13</sup>C NMR spectra of all synthesized intermediates and final compounds (PDF)

qNMR of synthesized compounds (PDF)

Molecular formula strings (CSV)

Modeling of AF and C inhibitors into SIRT2 (PDB)

## ■ AUTHOR INFORMATION

### Corresponding Author

\*E-mail: hl379@cornell.edu.

### ORCID

Ali Sohail Farooqi: 0000-0001-7763-6152

Hening Lin: 0000-0002-0255-2701

### Present Addresses

<sup>§</sup>Zhejiang Province Key Laboratory of Anti-Cancer Drug Research, College of Pharmaceutical Sciences, Zhejiang University, Hangzhou, China. 310058.

<sup>||</sup>Shanghai Institute of Materia Medica, Chinese Academy of Sciences, No. 501, Haik Rd., Pudong New District, Shanghai 201203, China.

### Author Contributions

A.S.F., J.Y.H., and J.C. contributed equally to this work. The manuscript was written through contributions of all authors. All authors have given approval to the final version of the manuscript.

### Funding

The work was supported by funds from HHMI and Cornell University. This work made use of the Cornell University NMR Facility, which is supported, in part, by the NSF through MRI award CHE-1531632. Imaging data was acquired through the Cornell University Biotechnology Resource Center, with NYSTEM (CO29155) and NIH (S10OD018516) funding for the shared Zeiss LSM880 confocal/multiphoton microscope.

### Notes

The authors declare the following competing financial interest(s): Cornell University has patent issued or pending on SIRT2 inhibitors.

## ■ ACKNOWLEDGMENTS

A.S.F. thanks Dr. Ying-Ling Chiang for his guidance in organic synthesis.

## ■ ABBREVIATIONS

BSA, bovine serum albumin; FBS, fetal bovine serum; LC–MS, liquid chromatography–mass spectrometry; HPLC, high performance liquid chromatography; PBS, phosphate buffered saline; DMSO, dimethyl sulfoxide; NAD<sup>+</sup>, nicotinamide adenine dinucleotide; TEA, triethylamine; TSA, Trichostatin A; TBS, Tris-buffered saline; NEAA, nonessential amino acids

## ■ REFERENCES

- (1) Houtkooper, R. H.; Pirinen, E.; Auwerx, J. Sirtuins as regulators of metabolism and healthspan. *Nat. Rev. Mol. Cell Biol.* **2012**, *13*, 225.
- (2) Imai, S.-i.; Armstrong, C. M.; Kaerberlein, M.; Guarente, L. Transcriptional silencing and longevity protein Sir2 is an NAD-dependent histone deacetylase. *Nature* **2000**, *403*, 795–800.
- (3) Bheda, P.; Jing, H.; Wolberger, C.; Lin, H. The substrate specificity of sirtuins. *Annu. Rev. Biochem.* **2016**, *85*, 405–429.
- (4) Chang, H.-C.; Guarente, L. SIRT1 and other sirtuins in metabolism. *Trends Endocrinol. Metab.* **2014**, *25*, 138–145.
- (5) Rodriguez, R. M.; Fernandez, A. F.; Fraga, M. F. Role of sirtuins in stem cell differentiation. *Genes Cancer* **2013**, *4*, 105–111.
- (6) Liu, P. Y.; Xu, N.; Malyukova, A.; Scarlett, C. J.; Sun, Y. T.; Zhang, X. D.; Ling, D.; Su, S.-P.; Nelson, C.; Chang, D. K.; Koach, J.; Tee, A. E.; Haber, M.; Norris, M. D.; Toon, C.; Rooman, I.; Xue, C.; Cheung, B. B.; Kumar, S.; Marshall, G. M.; Biankin, A. V.; Liu, T. The histone deacetylase SIRT2 stabilizes Myc oncoproteins. *Cell Death Differ.* **2013**, *20*, 503–514.
- (7) Song, N.-Y.; Surh, Y.-J. Janus-faced role of SIRT1 in tumorigenesis. *Ann. N.Y. Acad. Sci.* **2012**, *1271*, 10–19.
- (8) Xiangyun, Y.; Xiaomin, N.; linping, G.; Yunhua, X.; Ziming, L.; Yongfeng, Y.; Zhiwei, C.; Shun, L. Desuccinylation of pyruvate kinase M2 by SIRT5 contributes to antioxidant response and tumor growth. *Oncotarget* **2017**, *8*, 6984–6993.

- (9) Kim, H.-S.; Vassilopoulos, A.; Wang, R.-H.; Lahusen, T.; Xiao, Z.; Xu, X.; Li, C.; Veenstra, T. D.; Li, B.; Yu, H.; Ji, J.; Wang, X. W.; Park, S.-H.; Cha, Y. I.; Gius, D.; Deng, C.-X. SIRT2 maintains genome integrity and suppresses tumorigenesis through regulating APC/C activity. *Cancer Cell* **2011**, *20*, 487–499.
- (10) Jing, H.; Hu, J.; He, B.; Negrón Abril, Y. L.; Stupinski, J.; Weiser, K.; Carbonaro, M.; Chiang, Y.-L.; Southard, T.; Giannakakou, P.; Weiss, R. S.; Lin, H. A SIRT2-selective inhibitor promotes c-Myc oncoprotein degradation and exhibits broad anticancer activity. *Cancer Cell* **2016**, *29*, 297–310.
- (11) Jing, H.; Zhang, X.; Wisner, S. A.; Chen, X.; Spiegelman, N. A.; Linder, M. E.; Lin, H. SIRT2 and lysine fatty acylation regulate the transforming activity of K-Ras4a. *Elife* **2017**, *11*, e32436.
- (12) Zhou, W.; Ni, T. K.; Wronski, A.; Glass, B.; Skibinski, A.; Beck, A.; Kuperwasser, C. The SIRT2 deacetylase stabilizes Slug to control malignancy of basal-like breast cancer. *Cell Rep* **2016**, *17*, 1302–1317.
- (13) Outeiro, T. F.; Kontopoulos, E.; Altmann, S. M.; Kufareva, I.; Strathearn, K. E.; Amore, A. M.; Volk, C. B.; Maxwell, M. M.; Rochet, J.-C.; McLean, P. J.; Young, A. B.; Abagyan, R.; Feany, M. B.; Hyman, B. T.; Kazantsev, A. G. Sirtuin 2 Inhibitors Rescue -Synuclein-Mediated Toxicity in Models of Parkinson's Disease. *Science* **2007**, *317*, S16.
- (14) Lain, S.; Hollick, J. J.; Campbell, J.; Staples, O. D.; Higgins, M.; Aoubala, M.; McCarthy, A.; Appleyard, V.; Murray, K. E.; Baker, L.; Thompson, A.; Mathers, J.; Holland, S. J.; Stark, M. J. R.; Pass, G.; Woods, J.; Lane, D. P.; Westwood, N. J. Discovery, in vivo activity, and mechanism of action of a small-molecule p53 activator. *Cancer Cell* **2008**, *13*, 454–463.
- (15) Rumpf, T.; Schiedel, M.; Karaman, B.; Roessler, C.; North, B. J.; Lehotzky, A.; Oláh, J.; Ladwein, K. I.; Schmidtkunz, K.; Gajer, M.; Pannek, M.; Steegborn, C.; Sinclair, D. A.; Gerhardt, S.; Ovádi, J.; Schutkowski, M.; Sippl, W.; Einsle, O.; Jung, M. Selective Sirt2 inhibition by ligand-induced rearrangement of the active site. *Nat. Commun.* **2015**, *6*, 6263.
- (16) Spiegelman, N. A.; Price, I. R.; Jing, H.; Wang, M.; Yang, M.; Cao, J.; Hong, J. Y.; Zhang, X.; Aramsangtienchai, P.; Sadhukhan, S.; Lin, H. Direct comparison of SIRT2 inhibitors: potency, specificity, activity-dependent inhibition, and on-target anticancer activities. *ChemMedChem* **2018**, *13*, 1890–1894.
- (17) Cen, Y.; Sauve, A. A. Transition state of ADP-Ribosylation of acetyllysine catalyzed by *Archaeoglobus fulgidus* Sir2 determined by kinetic isotope effects and computational approaches. *J. Am. Chem. Soc.* **2010**, *132*, 12286–12298.
- (18) Hirsch, B. M.; Hao, Y.; Li, X.; Wesdemiotis, C.; Wang, Z.; Zheng, W. A mechanism-based potent sirtuin inhibitor containing N-thiocarbamoyl-lysine (TuAcK). *Bioorg. Med. Chem. Lett.* **2011**, *21*, 4753–4757.
- (19) Wang, Y.; Fung, Y. M. E.; Zhang, W.; He, B.; Chung, M. W. H.; Jin, J.; Hu, J.; Lin, H.; Hao, Q. Deacylation Mechanism by SIRT2 Revealed in the 1'-SH-2'-O-Myristoyl Intermediate Structure. *Cell Chem. Biol.* **2017**, *24*, 339–345.
- (20) Madsen, A. S.; Andersen, C.; Daoud, M.; Anderson, K. A.; Laursen, J. S.; Chakladar, S.; Huynh, F. K.; Colaço, A. R.; Backos, D. S.; Fristrup, P.; Hirschey, M. D.; Olsen, C. A. Investigating the sensitivity of NAD<sup>+</sup>-dependent sirtuin deacylation activities to NADH. *J. Biol. Chem.* **2016**, *291*, 7128–7141.
- (21) Michan, S.; Sinclair, D. Sirtuins in mammals: insights into their biological function. *Biochem. J.* **2007**, *404*, 1–13.
- (22) Guan, X.; Lin, P.; Knoll, E.; Chakrabarti, R. Mechanism of inhibition of the human sirtuin enzyme SIRT3 by nicotinamide: computational and experimental studies. *PLoS One* **2014**, *9*, No. e107729.
- (23) Avalos, J. L.; Bever, K. M.; Wolberger, C. Mechanism of sirtuin inhibition by nicotinamide: altering the NAD<sup>+</sup> cosubstrate specificity of a Sir2 enzyme. *Mol. Cell* **2005**, *17*, 855–868.
- (24) Kim, B. S.; Lee, C.-H.; Chang, G.-E.; Cheong, E.; Shin, I. A potent and selective small molecule inhibitor of sirtuin 1 promotes differentiation of pluripotent P19 cells into functional neurons. *Sci. Rep.* **2016**, *6*, 34324.
- (25) Solomon, J. M.; Pasupuleti, R.; Xu, L.; McDonagh, T.; Curtis, R.; DiStefano, P. S.; Huber, L. J. Inhibition of SIRT1 catalytic activity increases p53 acetylation but does not alter cell survival following DNA damage. *Mol. Cell. Biol.* **2006**, *26*, 28–38.
- (26) Teng, Y.-B.; Jing, H.; Aramsangtienchai, P.; He, B.; Khan, S.; Hu, J.; Lin, H.; Hao, Q. Efficient demyristoylase activity of SIRT2 revealed by kinetic and structural studies. *Sci. Rep.* **2015**, *5*, 8529.
- (27) Paoli, P.; Giannoni, E.; Chiarugi, P. Anoinis molecular pathways and its role in cancer progression. *Biochim. Biophys. Acta* **2013**, *1833*, 3481–3498.
- (28) Hanahan, D.; Weinberg, R. A. The hallmarks of cancer. *Cell* **2000**, *100*, S7–70.
- (29) Patel, S.; Pine, S.; Rameshwar, P. Noble Agar Assay for Self-Renewal. *Protoc. Exch.* **2013**, DOI: 10.1038/protex.2013.021.
- (30) North, B. J.; Marshall, B. L.; Borra, M. T.; Denu, J. M.; Verdine, E. The human Sir2 ortholog, SIRT2, is an NAD<sup>+</sup>-dependent tubulin deacetylase. *Mol. Cell* **2003**, *11*, 437–444.
- (31) Vaziri, H.; Dessain, S. K.; Eaton, E. N.; Imai, S.-I.; Frye, R. A.; Pandita, T. K.; Guarente, L.; Weinberg, R. A. hSIR2SIRT1 Functions as an NAD-Dependent p53 Deacetylase. *Cell* **2001**, *107*, 149–159.
- (32) Gertz, M.; Fischer, F.; Nguyen, G. T. T.; Lakshminarasimhan, M.; Schutkowski, M.; Weyand, M.; Steegborn, C. Ex-527 inhibits sirtuins by exploiting their unique NAD<sup>+</sup>-dependent deacetylation mechanism. *Proc. Natl. Acad. Sci. U.S.A.* **2013**, *110*, No. E2772.
- (33) Moriarity, A.; O'Sullivan, J.; Kennedy, J.; Mehigan, B.; McCormick, P. Current targeted therapies in the treatment of advanced colorectal cancer: a review. *Ther. Adv. Med. Oncol.* **2016**, *8*, 276–293.
- (34) El Zouhairi, M.; Charabaty, A.; Pishvaian, M. J. Molecularly targeted therapy for metastatic colon cancer: proven treatments and promising new agents. *Gastrointest. Cancer Res.* **2011**, *4*, 15–21.
- (35) Lièvre, A.; Bachet, J.-B.; Boige, V.; Cayre, A.; Le Corre, D.; Buc, E.; Ychou, M.; Bouché, O.; Landi, B.; Louvet, C.; André, T.; Bibeau, F.; Diebold, M.-D.; Rougier, P.; Ducreux, M.; Tomasic, G.; Emile, J.-F.; Penault-Llorca, F.; Laurent-Puig, P. KRAS Mutations As an Independent Prognostic Factor in Patients With Advanced Colorectal Cancer Treated With Cetuximab. *J. Clin. Oncol.* **2008**, *26*, 374–379.
- (36) Hsu, H.-C.; Thiam, T. K.; Lu, Y.-J.; Yeh, C. Y.; Tsai, W. S.; You, J. F.; Hung, H. Y.; Tsai, C.-N.; Hsu, A.; Chen, H.-C.; Chen, S.-J.; Yang, T.-S. Mutations of KRAS/NRAS/BRAF predict cetuximab resistance in metastatic colorectal cancer patients. *Oncotarget* **2016**, *7*, 22257–22270.
- (37) Raponi, M.; Winkler, H.; Dracopoli, N. C. KRAS mutations predict response to EGFR inhibitors. *Curr. Opin. Pharmacol.* **2008**, *8*, 413–418.